Stereo Particle Image Velocimetry Measurements of Transition Downstream of a Backward-Facing Step in a Swept-Wing Boundary Layer

Jenna L. Eppink* and Chung-Sheng Yao*
NASA Langley Research Center, Hampton, VA 23681

Stereo particle image velocimetry measurements were performed downstream of a backward-facing step in a stationary-crossflow dominated flow. The PIV measurements exhibit excellent quantitative and qualitative agreement with the previously acquired hotwire data. Instantaneous PIV snapshots reveal new information about the nature and cause of the "spikes" that occurred prior to breakdown in both the hotwire and PIV data. The PIV snapshots show that the events occur simultaneously across multiple stationary crossflow wavelengths, indicating that this is not simply a local event, but is likely caused by the 2D Tollmien-Schlichting instability that is introduced by the step. While the TS instability is a 2D instability, it is also modulated in the spanwise direction due to interactions with the stationary crossflow, as are the other unsteady disturbances present. Because of this modulation, the "spike" events cause an instantaneous increase of the spanwise modulation of the streamwise and spanwise velocity initially caused by the stationary crossflow. Breakdown appears to be caused by this instantaneous modulation, possibly due to a high-frequency secondary instability similar to a traveling-crossflow breakdown scenario. These results further illuminate the respective roles of the stationary crossflow and unsteady disturbances in transition downstream of a backward-facing step.

Nomenclature

C_p	Pressure coefficient, $C_p = \frac{p-p_\infty}{\frac{1}{2}\rho U_\infty^2}$
f	frequency
h	step height
Re'	Unit Reynolds number
Tu	turbulence intensity
U', V', W'	steady disturbance velocity
u', v', w'	fluctuating components of velocity
U'_{rms}	spanwise root mean square of steady disturbance velocity, U'
U, V, W	velocity components in the x, y, and z' directions
U_e	boundary layer edge velocity
U_∞	freestream velocity
x	streamwise direction
x_h	streamwise location of step
x_r	reattachment location in terms of the number of step heights downstream of the step
x_{sh}	number of step heights downstream of step
y	wall-normal direction
z	spanwise direction (parallel to the leading edge)
z'	direction normal to side-wall

*Research Aerospace Engineer, Flow Physics and Control Branch, M.S. 170, AIAA Member

Symbols

δ	boundary layer thickness
λ_z	spanwise wavelength

I. Introduction

LAMINAR flow control remains a promising technique for improving the fuel efficiency of aircraft in the near future. In theory and in the laboratory, laminar flow control (LFC) techniques can work quite well. However, real-world applications result in additional difficulties that can be detrimental if not well-managed. One such difficulty is the disruption of laminar flow that can occur if small protuberances or surface imperfections are present on the wing surface. These imperfections can result from insect residue, rivets, bolts, steps, gaps, paint, and other sources. In order for LFC to be effective in an operational environment, it is crucial that we gain a better understanding of how surface irregularities affect transition. This is important so that more reasonable manufacturing tolerances can be specified.

In a swept-wing flow, stationary crossflow is typically the dominant transition mechanism. However, when a step is introduced into the flow, the step can act as a receptivity site for other types of disturbances, and it can also modify the mean flow so that those disturbances are destabilized for a short region downstream of the step.

The effect of 2D steps on swept-wing transition has been studied recently. This work has generally been limited to observing the behavior of the transition front as the step height is increased,[1,2] but more recently, researchers have begun to study the flow in more detail. Eppink et al.[3] reported detailed boundary-layer measurements downstream of a backward-facing step and identified several different types of instabilities that were introduced by the step and modulated by the stationary crossflow vortices. One of the unsteady disturbances identified downstream of the step is believed to be a traveling crossflow instability, similar to what was seen in the computations of Tufts et al.[4] Duncan et al.[5] performed hotwire measurements downstream of forward- and backward-facing steps to determine the effect of the steps on stationary crossflow instabilities. They found that the steps caused an increase in N-factor for the stationary crossflow, but the stationary crossflow amplitudes were very low at the step, and therefore, the uncertainty of the N-factors was high. Tufts et al.[4] performed computations to study the interaction between stationary crossflow instabilities and a two-dimensional step excrescence. They found that the backward-facing step did not amplify the stationary crossflow modes, but they did verify the existence of a traveling instability in the recirculation region downstream of the step. They concluded that transition is likely caused by an interaction between this traveling mode and the stationary crossflow mode. Saeed et al.[6] performed measurements downstream of strips of varying heights and locations. While the mechanism is expected to be somewhat different, since the flow first encounters a forward-facing step, followed by a backward-facing step, some of the results are similar to those seen downstream of a pure backward-facing step. For instance, a higher level of unsteady disturbances is encountered as the height of the excrescence is increased, and the unsteadiness introduced by the step covers a broad band of frequencies.

Transition over protuberances (such as 2D steps) is complicated and apparently involves the interaction of multiple types of disturbances. The current research is a follow-on experiment to the hotwire results described by Eppink et al.[3] Stereo particle image velocimetry (SPIV) measurements are undertaken in order to gain a better understanding of the breakdown mechanism leading to transition downstream of a backward-facing step.

II. Experimental Setup

The experiment was performed in the 2-Foot by 3-Foot Low Speed Boundary-Layer Channel at the NASA Langley Research Center. The tunnel is a closed circuit facility with a 0.61-m high by 0.91-m wide by 6.1-m long test section. The tunnel can reach speeds up to 45 m/s (unit Reynolds number, $Re' = 2.87 \times 10^6$/m) in the test section. Freestream turbulence intensity levels, $Tu = \frac{1}{U_\infty}\sqrt{\frac{1}{3}(u'^2 + v'^2 + w'^2)}$, were measured using a crosswire in an empty test section to be less than 0.06% for the entire speed range of the tunnel, and less than 0.05% for the test speed of 26.5 m/s. This value represents the total energy across the spectrum, high-pass filtered at 0.25 Hz. Thus, this tunnel can be considered a low-disturbance facility for purposes of conducting transition experiments.[7]

The 0.0127-m thick flat plate model consists of a 0.41-m long leading-edge piece, swept at 30°, and a larger downstream piece (see Fig. 1). The model is 0.91 m wide (thus, spanning the width of the test section) and 2.54 m long on the longest edge. The downstream or leading edge pieces can be adjusted relative to each other using precision shims to create either forward-facing or backward-facing 2D steps of different heights, parallel with the leading edge. The leading edge piece was polished to a surface finish of 0.2 μm, and the larger downstream plate had a surface finish of 0.4 μm. A leading-edge contour was designed for the bottom side of the plate in order to make the suction-peak less severe, and therefore avoid separation, which could potentially cause unsteadiness in the attachment line.

A 3D pressure body along the ceiling was designed to induce a streamwise pressure gradient, which, along with the sweep, causes stationary crossflow growth. A second purpose of the ceiling liner was to simulate infinite swept-wing flow within a midspan measurement region of width 0.3 meters. This was achieved by designing the liner such that the C_p contours were parallel with the leading edge within the measurement region. The ceiling liner was fabricated out of a hard foam using a computer-controlled milling machine.

All measurements were performed at a freestream velocity of 26.5 m/s ($Re' = 1.69$ x 10^6/m). The current experiment utilized a single leading-edge roughness configuration consisting of discrete roughness elements (DREs) with a diameter of 4.4 mm. The DREs were applied with a spanwise spacing, λ_z, of 11 mm and were approximately 20 μm thick. The spacing of the DREs (11 mm) corresponds to the most amplified stationary crossflow wavelength calculated for the baseline case with no step. For more details of the experiment setup, refer to Eppink.[8]

A 200 mJ double-pulsed Nd:YAG laser provided the laser sheet for the SPIV measurements. The laser sheet was set up as a y-z' plane, perpendicular to the freestream flow direction (see Fig. 1). Ideally, the measurements would be performed in a plane parallel with the step, and thus, the laser sheet would need to be parallel with the step. It was not possible to get the light sheet parallel with the step due to optical limitations with the current setup, but modifications are planned to allow this improvement for future measurements. One drawback of the current setup is the inability to make measurements close to the step since the laser sheet will burn the model when it hits the backside of the backward-facing step. Two 2 megapixel cameras were placed on the outboard side of the test section at a 45° angle to the laser sheet. To achieve the desired field of view and resolution, 300 mm lenses were utilized, resulting in a measurement area of approximately 30 mm x 30 mm. This area allows acquisition of three wavelengths of the stationary crossflow instability in a single frame, while still acquiring approximately 20 points (using 50% overlap of the interrogation area) inside the boundary layer. The cameras and laser are all mounted on the same traversing system, which allowed measurements at multiple locations with relative ease. An oil-based fog machine generated the seeding, which was introduced downstream of the test section.

III. Previous Experimental Results

Hotwire results for the backward-facing step (BFS) cases are discussed in detail by Eppink et al.[3] but will be summarized here as context for the following discussion. Measurements were performed with and without DREs on the leading edge of the model. In all cases, transition occurred far downstream and was dominated by stationary crossflow until the step height was increased above approximately 49% of the local boundary-layer thickness (δ) for the baseline case. At that step height, transition moved upstream abruptly, but still occurred more than 300 step heights downstream of the step. This was also well downstream of the separation bubble, which extended approximately 30 step heights downstream of the step. The velocity spectra downstream of the step were found to be rich with unsteady disturbances in a broad frequency band ($f \approx 80$ to 1500 Hz). These unsteady disturbances were not present in the baseline case and are believed to be directly responsible for transition in the presence of the step since the stationary crossflow amplitudes remained too low to cause transition via their high-frequency secondary instabilities. Data were acquired simultaneously from two hotwires in the boundary layer to extract phase speed and wave angle information. Based on these results, three distinct disturbance bands were identified corresponding to a traveling crossflow (TCF) type disturbance (f=80 to 200 Hz), a Tollmien-Schlichting (TS) disturbance (f=200 to 800 Hz), and a shear-layer disturbance (f=800 to 1500 Hz). The linear stability calculations performed for the baseline case did not show the existence of any unstable TS modes due to the favorable pressure gradient. The existence of this instability in the experiment is believed to be due to the short unfavorable pressure gradient region that exists downstream of the BFS. The TS instabilities may be unstable in this short region, and then persist downstream due to nonlinear interactions.

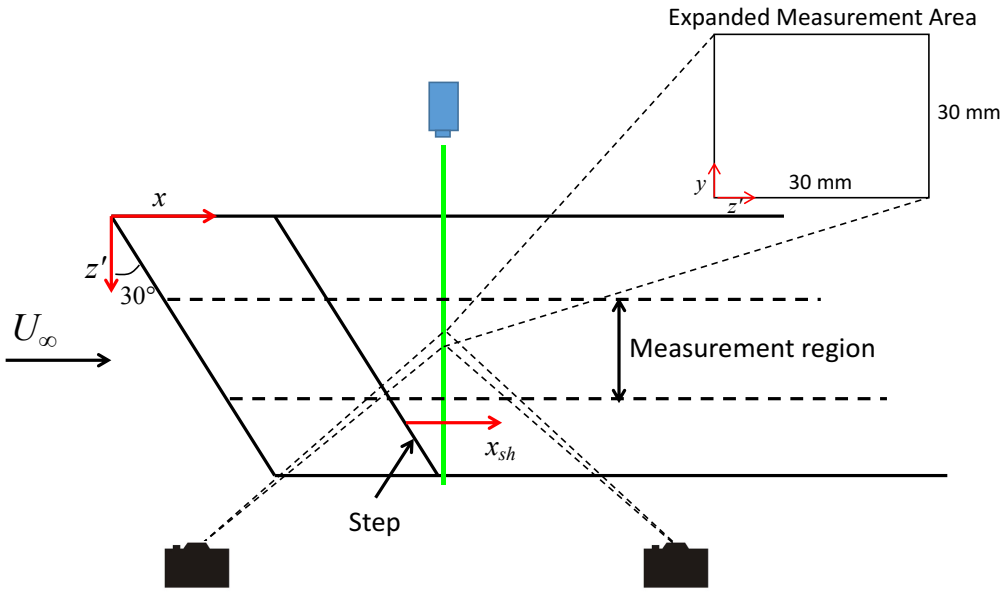

Figure 1: Top view of PIV setup.

The unsteady disturbances were modulated in the spanwise direction by the stationary crossflow and thus formed regions of peaks and valleys in amplitude with spanwise spacing corresponding to the dominant stationary crossflow wavelength. Large spikes in velocity were observed to occur well upstream of the breakdown location and appeared to be related to some type of breakdown mechanism resulting from the unsteady disturbances. The hotwire time trace in Fig. 2a shows an example of a location that was experiencing a large number of positive velocity spikes. Regions of positive and negative spikes occurred with spanwise spacing related to the stationary crossflow wavelength of 11 mm. Positive spikes occurred near the wall while the negative spikes occurred off the wall and offset spanwise from the positive spikes. This is illustrated in Fig. 2b, in which positive skewness indicates the occurrence of positive spikes, and negative skewness indicates negative spikes. SPIV measurements were undertaken to further study the spike breakdown mechanism. These measurements were performed for the backward-facing step height of 1.14 mm (45% δ).

IV. SPIV Results

The SPIV results compare well with the previously acquired single-hotwire data. Results for the spanwise-averaged boundary layer profile and the steady U-perturbation profiles at $x_{sh} \approx 100$ are shown in Fig. 3. The boundary-layer profiles show excellent agreement (Fig. 3a). The U-perturbation profiles are obtained by integrating the wavelength spectra of U at each wall-normal location from $\lambda_z \approx 8$ to 20 mm. These profiles agree fairly well, though there is some minor discrepancy in the amplitude and height of the peak (Fig. 3b). In addition to the agreement of these measurements, we observed similar qualitative behavior for the hotwire and PIV results throughout all of the measurements made thus far. For instance, the location and appearance of the spikes are consistent between the two measurement techniques. This is noteworthy because it indicates that the particles that are introduced into the flow to enable the PIV measurements do not have a significant impact on the transition behavior.

SPIV measurements were performed at several stations downstream of the step with DREs on the leading edge. The most upstream measurement was performed at $x_{sh} \approx 98$, while the farthest downstream measurement was made at approximately x_{sh}=296. Breakdown to turbulence appears to begin at approximately x_{sh}=185.

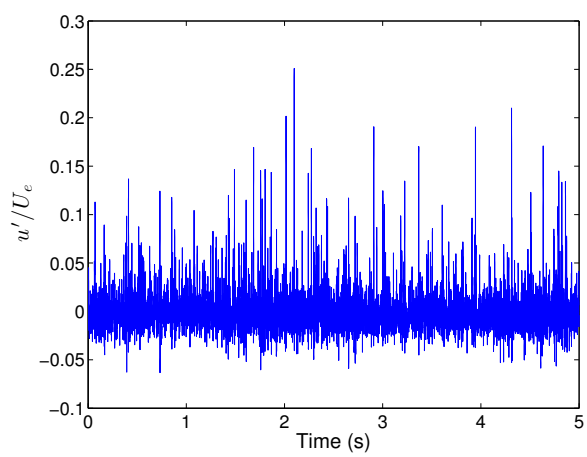

(a) **Hotwire time trace in boundary layer showing positive velocity spikes.**

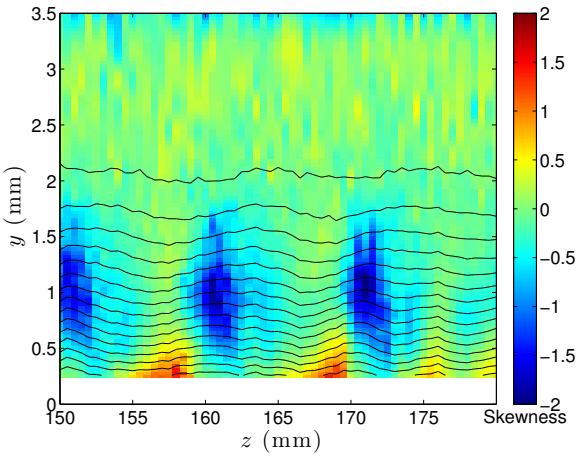

(b) **Skewness (colors) and mean flow (lines) contours at a plane downstream of the step.**

Figure 2: Results from hotwire campaign showing measurements of the spike breakdown mechanism.

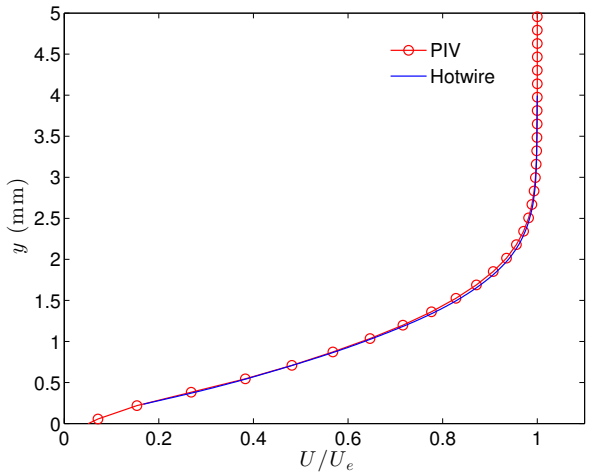

(a) **Comparison of PIV and hotwire measurements of mean velocity profile at $x_{sh} \approx 100$.**

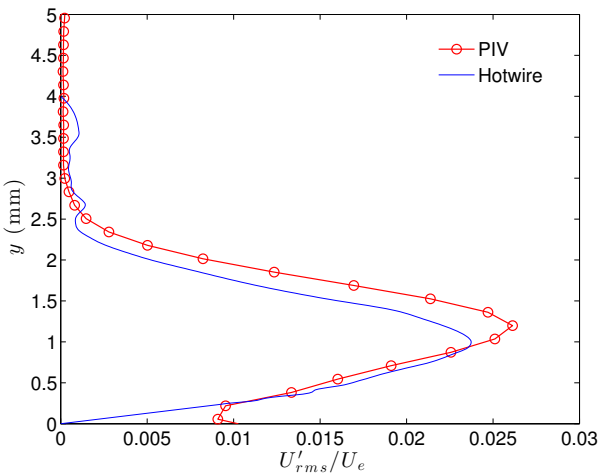

(b) **Comparison of PIV and hotwire measurements of U-perturbation profile (U'_{rms}) at $x_{sh} \approx 100$.**

Figure 3: Comparison of hotwire and PIV measurements at $x_{sh} \approx 100$.

One major advantage of PIV measurements over hotwire measurements is the ability to acquire instantaneous snapshots of an entire plane of data. The results immediately shed more light on the nature of the spike breakdown mechanism that was seen from the hotwire results. Fig. 4 illustrates this advantage. The plot on the bottom (Fig. 4c) shows the streamwise velocity at a single point in the boundary layer (indicated by the black dot) for each of the 1000 image pairs acquired. The two figures on the top show the instantaneous streamwise velocity field during a spike sample (Fig. 4a) and a nonspike sample (Fig. 4b). It is immediately apparent that the "spike" event is not a local phenomenon, but is occurring simultaneously over multiple stationary crossflow wavelengths. Additionally, it results in an instantaneous increase in the spanwise modulation of the streamwise velocity.

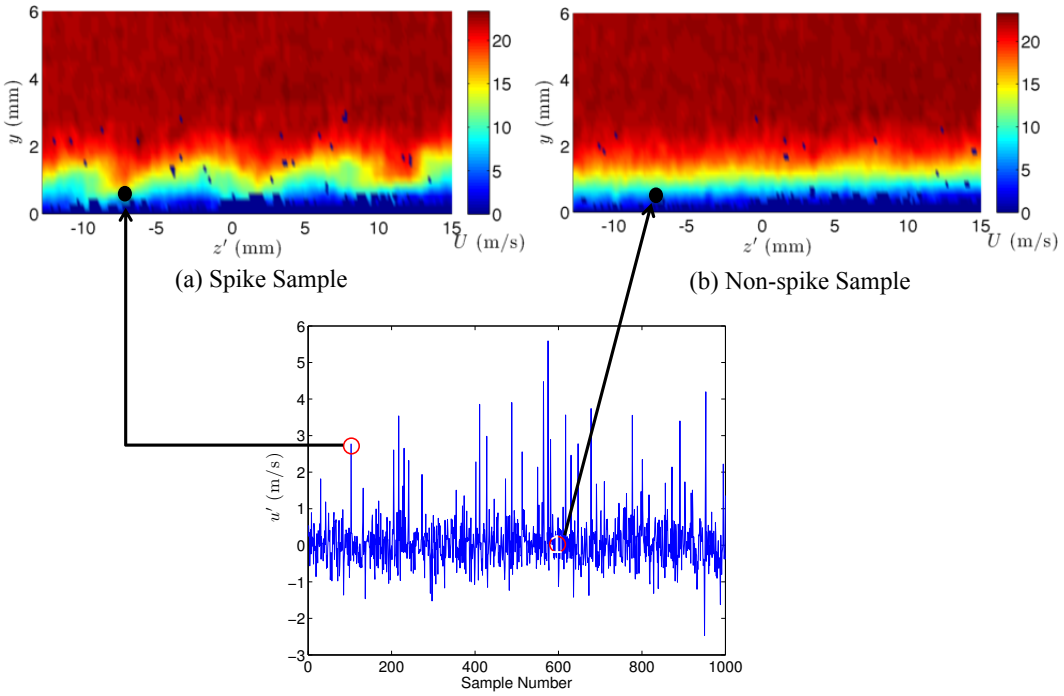

Figure 4: Instantaneous PIV snapshots at $x_{sh} \approx 120$ showing spike and nonspike samples.

These results provide some clues about the origin of the spikes. As noted earlier, the large amplitude modulation that occurs during a spike event is created across multiple wavelengths of the stationary crossflow simultaneously. This behavior indicates that the disturbance has a two-dimensional nature associated with it, even though the effect on the flow field appears to be three-dimensional. This indicates that the spikes are occurring at least partially due to an interaction between the TS wave, which is a 2D instability, and the stationary crossflow. The stationary crossflow modulates the TS wave, causing regions of enhanced fluctuation amplitude across the span. The stationary crossflow also distorts the wavefront of the TS wave. Both of these effects are illustrated by Eppink et al.[9] using phase-averaged hotwire results. Since the spikes occur only positive and negative in certain locations, as shown in Fig. 2b, there is likely another interaction taking place to cause this behavior, possibly with the lower frequency traveling-crossflow instabilities.

The effect of the spikes on the spanwise modulation of the velocity is investigated further by averaging together all of the "spike" and "nonspike" samples. A single measurement is considered a "spike" sample if the disturbance velocity (u') at the point indicated in Fig. 4 ($z' \approx -7$ mm, $y \approx 0.7$ mm) is greater than 2 m/s. A measurement is considered a "nonspike" sample if the u' value at this point is between -0.5 and 0.5 m/s. These threshold values are somewhat arbitrary, but the results are not sensitive to small changes in these values. The results from this analysis, shown in Fig. 5, look similar to the instantaneous results shown in Fig. 4. Results are shown for two locations: x_{sh}=98, and x_{sh}=164. While there is some mean flow modulation evident in the nonspike average due to the presence of the stationary crossflow, the modulation is much larger when the spike events are averaged together. The amplitude of the modulation is similar between the two stations shown, but the shape of the modulation changes as we progress downstream.

Note that if we perform this same exercise for a location at which negative spikes occur, we obtain similar results. Similarly, the spanwise velocity (W) is plotted for the "spike" and "nonspike" samples in Fig. 6. During the spike events, not only is the modulation increased, but the negative amplitude of the spanwise velocity is increased near the locations of the positive spikes.

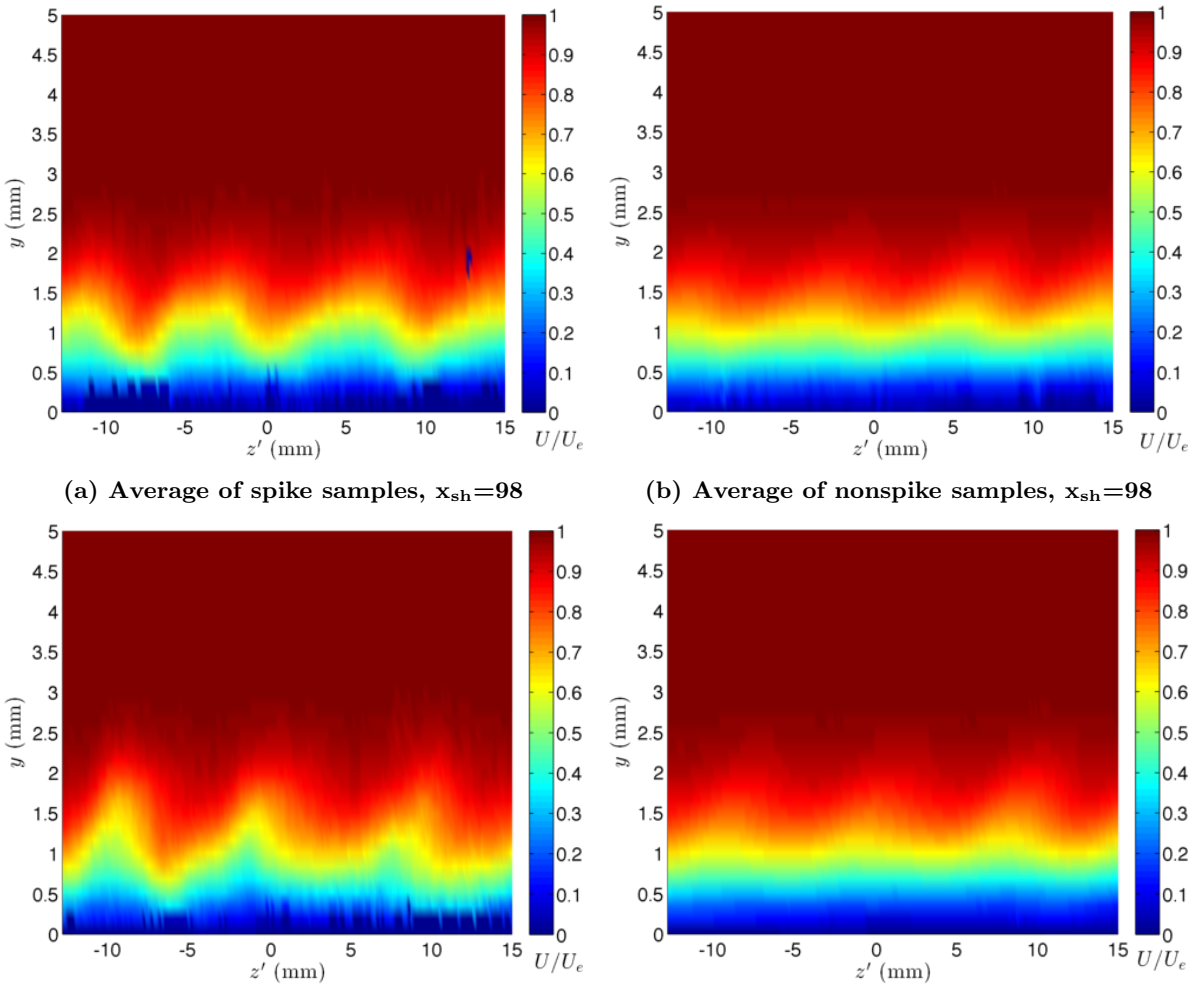

(a) Average of spike samples, x_{sh}=98

(b) Average of nonspike samples, x_{sh}=98

(c) Average of spike samples, x_{sh}=164

(d) Average of nonspike samples, x_{sh}=164

Figure 5: Average of streamwise velocity (U) for spike and nonspike samples.

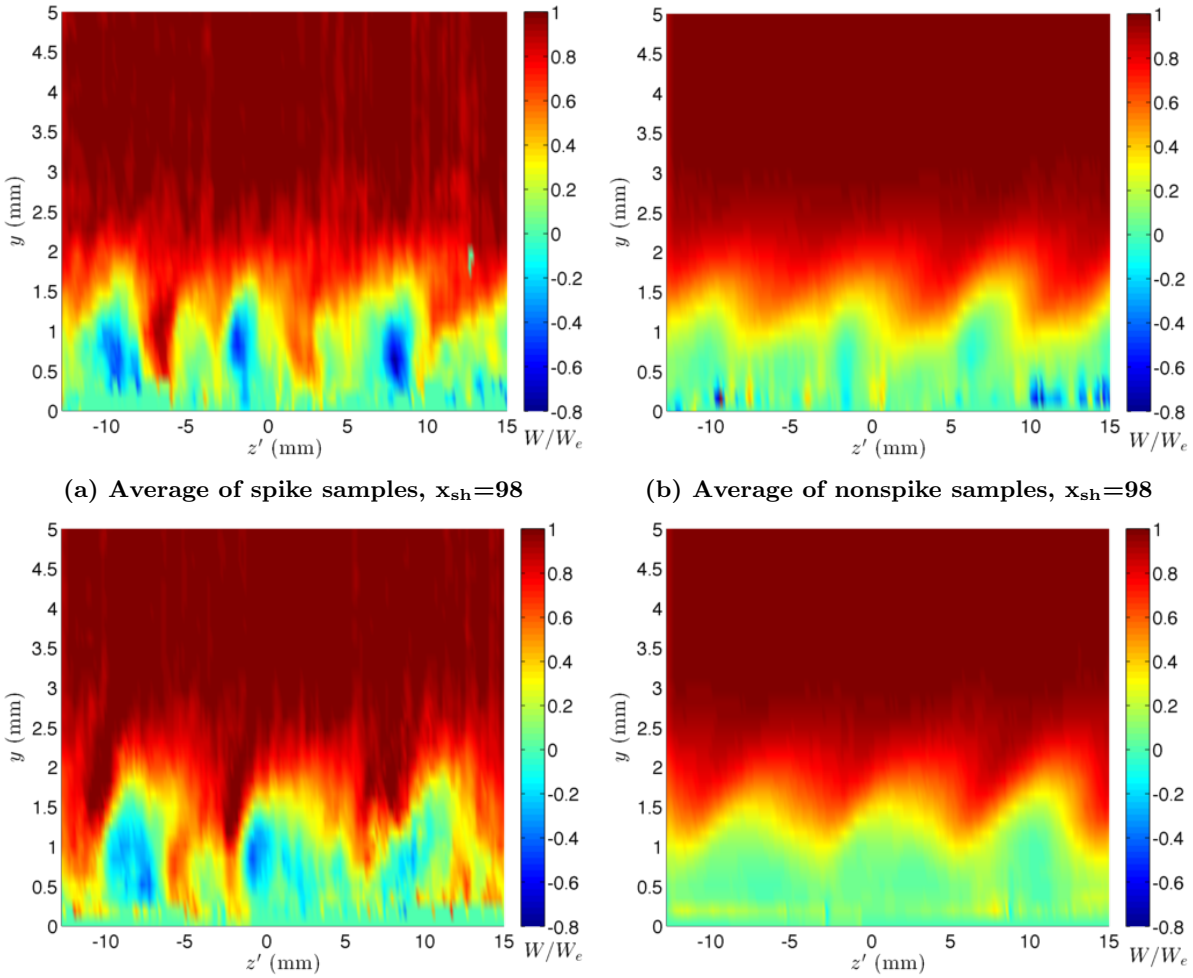

(a) Average of spike samples, x_{sh}=98

(b) Average of nonspike samples, x_{sh}=98

(c) Average of spike samples, x_{sh}=164

(d) Average of nonspike samples, x_{sh}=164

Figure 6: Average of spanwise velocity (W) for spike and nonspike samples.

Figure 7 shows the steady U-perturbation profiles for the averaged spike and nonspike samples. During the spike samples, the amplitude of the spanwise modulation of the streamwise velocity is approximately 2 times larger than during the nonspike samples. These results indicate that in this case, breakdown may be occurring intermittently as a result of the instantaneous modulation of the streamwise velocity, possibly due to the occurrence of a high-frequency secondary instability. It is well known that high-frequency secondary instabilities cause breakdown in the case of a flow dominated by stationary or traveling crossflow instabilities.[10–15] The secondary instabilities are destabilized by the high spanwise or wall-normal shear that occurs locally when the flow becomes highly modulated by the crossflow instabilities. In the case of traveling crossflow, this modulation occurs instantaneously. The current breakdown scenario may be similar to that of traveling crossflow, but in this case, it does not appear to be traveling crossflow that is causing the instantaneous modulation of the flow. There is evidence in the hotwire data of high-frequency oscillations occurring during the spike events, examples of which are shown in Fig. 8. The frequency range of this content is within the expected range for the high-frequency secondary instabilities ($f \approx 2000$ to 5000 Hz). It is still not clear where this "spike" mechanism is originating from, but it is now evident that crossflow instabilities may play an important role in the breakdown of flow over a swept backward-facing step.

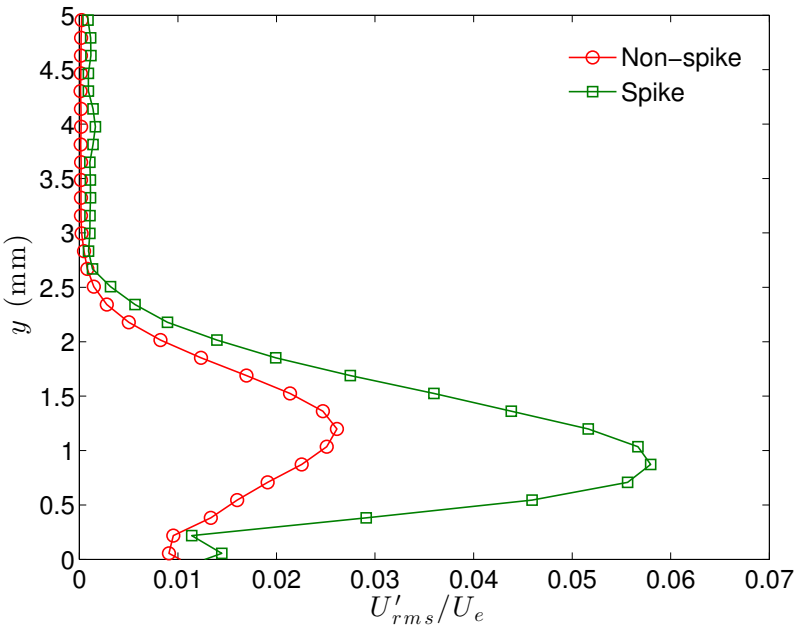

Figure 7: Stationary crossflow mode-shapes at x_{sh}=98.

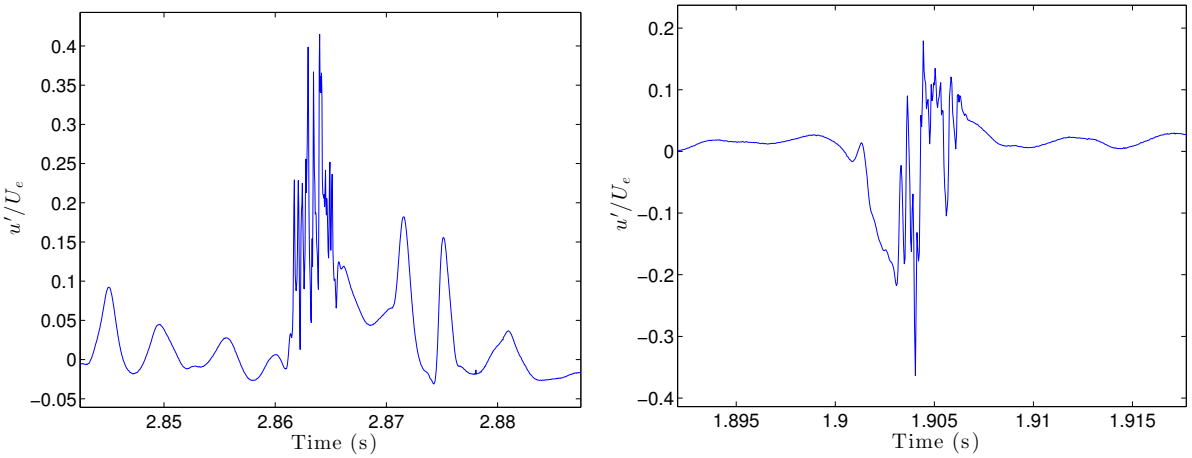

(a) Positive spike **(b) Negative spike**

Figure 8: Example hotwire data showing high-frequency content during positive and negative spike events.

Instantaneous snapshots at several streamwise stations are shown in Fig. 9 to illustrate the evolution and breakdown of the boundary layer during the spike events. From x_{sh}=98 to 140 (Figs. 9a-9b), the velocity contours appear very similar during these events. By x_{sh}=164 (Fig. 9c), the modulation of the flow is very large, and some smaller wavelength (possibly harmonic) content is present. The last three stations (Figs. 9d-9f) show the beginning of breakdown, as the larger structures start to break up and smaller scale structures start to appear.

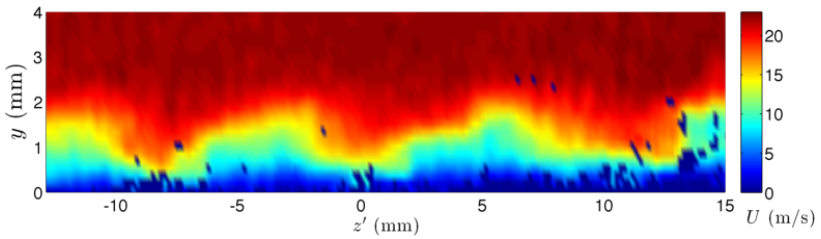

(a) $\mathbf{x_{sh}}$=98

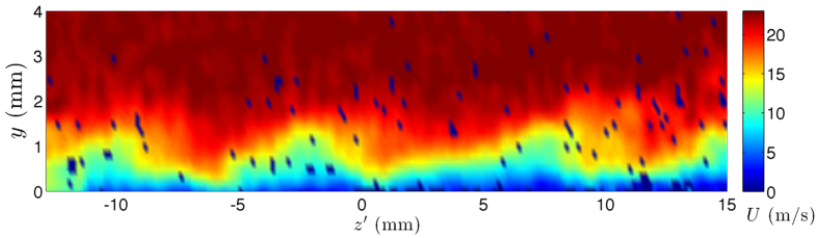

(b) $\mathbf{x_{sh}}$=140

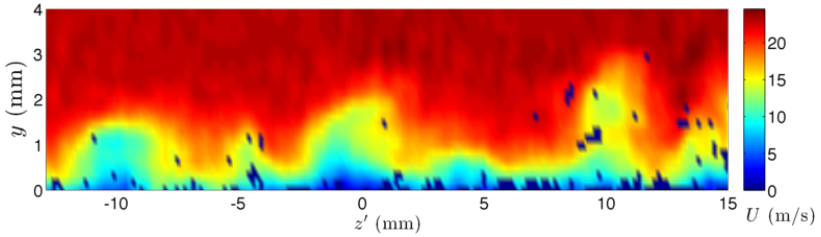

(c) $\mathbf{x_{sh}}$=164

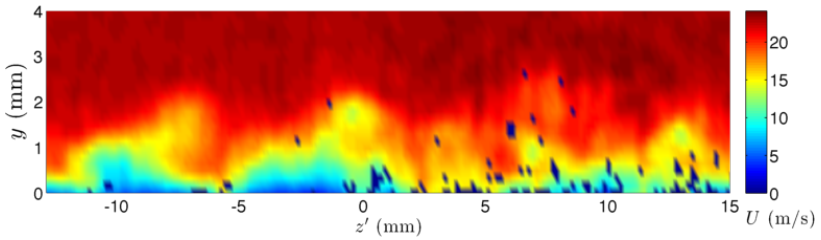

(d) $\mathbf{x_{sh}}$=185

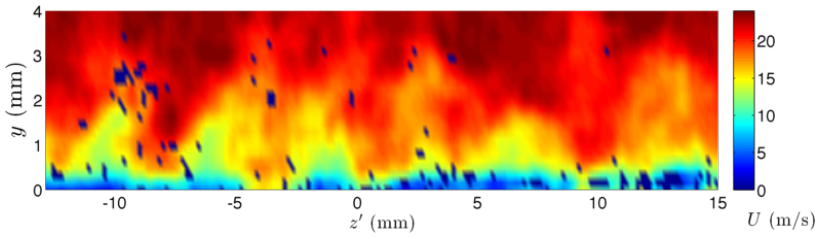

(e) $\mathbf{x_{sh}}$=227

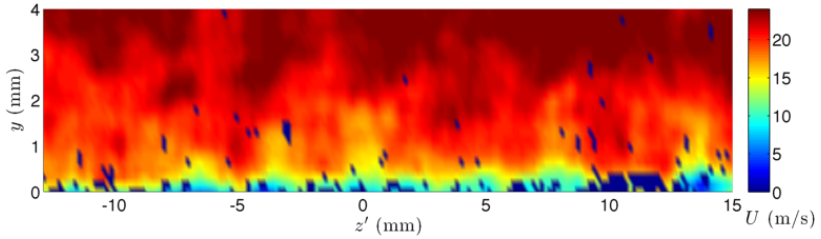

(f) $\mathbf{x_{sh}}$=248

Figure 9: PIV snapshots of streamwise velocity (U) for spike samples.

V. Summary and Concluding Remarks

Stereo particle image velocimetry measurements were performed downstream of a backward-facing step in a stationary-crossflow dominated boundary layer. The SPIV results reveal details about the transition mechanisms that are not possible to deduce from the hotwire measurements. The SPIV measurements agreed well with the hotwire results, indicating that the particles introduced into the flow do not have a significant impact on transition.

This study focused on the "spike" mechanism that was observed in both the hotwire and PIV data to occur prior to breakdown. Two important observations are made from the SPIV results regarding this spike mechanism. The first observation is that the negative spikes and positive spikes, which were observed in the hotwire data at different spatial locations, occur at approximately the same time. This means that the spanwise modulation of the flow, which is initially caused by the stationary crossflow, is instantaneously increased. At the streamwise locations measured in this study, the modulation was increased by approximately a factor of two. This, along with data from the hotwire campaign, indicates that breakdown possibly occurs via high-frequency secondary instabilities resulting from the instantaneous modulation of the flow during these spike events.

The second observation is that the spike events happen simultaneously across multiple wavelengths of the stationary crossflow wavelength. This behavior indicates that the spikes originate from a 2D disturbance, likely the TS disturbance identified from the hotwire data. As observed in earlier studies, the initially 2D TS wave is modulated by the stationary crossflow, resulting in regions of peaks and valleys in fluctuation amplitude. The stationary crossflow also distorts the wavefront of the TS wave, causing negative and positive parts of the phase to pass through the plane simultaneously. This behavior results in an instantaneous distortion of the flow in the spanwise plan, with a wavelength matching that of the stationary crossflow. Thus, the TS appears to play a strong role in the generation of these spike events, but it is probably not the only player, and there are likely some other interactions going on. We hope to further illuminate these interactions with future studies using time-resolved PIV.

VI. Acknowledgments

This work was performed as part of the Revolutionary Computational Aerosciences discipline under the Transformational Tools and Technologies Project of the NASA Fundamental Aeronautics Program. The authors would like to thank Mark Fletcher and Charles Debro for their support of the laser setup and wind tunnel testing, and the members of the Flow Physics and Control Branch of the NASA Langley Research Center for their support and many helpful discussions.

References

[1]Perraud, J. and Seraudie, A., "Effects of Steps and Gaps on 2D and 3D Transition," *European Congress on Comp. Methods in Applied Science and Eng., ECCOMAS*, 2000, pp. 11–14.

[2]Duncan Jr, G., Crawford, B., and Saric, W., "Effects of Step Excrescences on Swept-Wing Transition," AIAA Paper 2013-2412, 2013.

[3]Eppink, J., Wlezien, R., King, R., and Choudhari, M., "The Interaction of Stationary Crossflow and a Backward-facing Step in Swept Boundary-Layer Transition," AIAA Paper 2015-0273, 2015.

[4]Tufts, M. W., Reed, H. L., Crawford, B. K., Duncan Jr, G. T., and Saric, W. S., "Computational Investigation of Step Excrescence Sensitivity in a Swept-Wing Boundary Layer," AIAA Paper 2015-2775, 2015.

[5]Duncan Jr, G. T., Crawford, B. K., Tufts, M. W., Saric, W. S., and Reed, H. L., "Effects of Step Excrescences on a Swept Wing in a Low-Disturbance Wind Tunnel," AIAA Paper 2014-0910, 2014.

[6]Saeed, T. I., Mughal, M. S., and Morrison, J., "The Interaction of a Swept-Wing Boundary Layer with Surface Excrescences," AIAA Paper 2016-2065, 2016.

[7]Saric, W. S. and Reshotko, E., "Review of Flow Quality Issues in Wind Tunnel Testing," AIAA Paper 1998-2613, 1998.

[8]Eppink, J., *The Interaction of Crossflow Instabilities and a Backward-Facing Step in Swept Boundary Layer Transition*, Ph.D. thesis, Tufts University, 2014.

[9]Eppink, J. L., Shishkov, O., Wlezien, R. W., King, R. A., and Choudhari, M., "The Effect of Acoustic Forcing on Instabilities and Breakdown in Swept-Wing Flow Over a Backward-Facing Step," AIAA Paper 2016-2063, 2016.

[10]Kohama, Y., Saric, W., and Hoos, J., "A High-Frequency, Secondary Instability of Crossflow Vortices that Leads to Transition," *Proc. of the Royal Aero. Soc. Conf.*, 1991, pp. 1–12.

[11]Malik, M., Li, F., and Chang, C.-L., "Crossflow Disturbances in Three-Dimensional Boundary Layers:Nonlinear Development, Wave Interaction and Secondary Instability," *Journal of Fluid Mechanics*, Vol. 268, No. 1, 1994, pp. 1–36.

[12]Malik, M. R., Li, F., Choudhari, M. M., and Chang, C.-L., "Secondary Instability of Crossflow Vortices and Swept-Wing Boundary-Layer Transition," *Journal of Fluid Mechanics*, Vol. 399, 1999, pp. 85–115.

[13]White, E. and Saric, W., "Secondary Instability of Crossflow Vortices," *Journal of Fluid Mechanics*, Vol. 525, No. 1, 2005, pp. 275–308.

[14]Duan, L., Choudhari, M. M., and Li, F., "Direct Numerical Simulation of Transition in a Swept-Wing Boundary Layer," AIAA Paper 2013-2617, 2013.

[15]Li, F., Choudhari, M. M., and Duan, L., "Direct Numerical Simulation of Transition due to Traveling Crossflow Vortices," AIAA Paper 2015-2771, 2015.